J Mater Sci (2009) 44:6470–6483
DOI 10.1007/s10853-009-3630-5

MESOSTRUCTURED MATERIALS

Transformation of microporous titanium glycolate nanorods into mesoporous anatase titania nanorods by hot water treatment

Srinivasan Priya · Jacques Robichaud · Marie-Claude Méthot · Subramanian Balaji · James M. Ehrman · Bao-Lian Su · Yahia Djaoued

Received: 29 November 2008 / Accepted: 19 May 2009 / Published online: 9 June 2009

Abstract High surface area titanium glycolate microporous multi-faceted nanorods were synthesized from the reaction of titanium alkoxides ($Ti(OEt)_4$, $Ti(O^iPr)_4$, or $Ti(O^nBu)_4$) with ethylene glycol, using a sol–gel reflux method. The specific surface area of the as-synthesized titanium glycolate nanorods obtained from $Ti(OEt)_4$ is $\sim$480 m^2/g. A hot water treatment at 90 °C for 1 h transformed the titanium glycolate microporous nanorods into mesoporous anatase TiO_2 nanorods. The shape of the nanorods was conserved after hot water treatment and the microporous to mesoporous transformation took place without significant change in the surface area (477 m^2/g). Micro Raman spectroscopy, scanning electron microscopy, transmission electron microscopy, X-ray diffraction, solid state NMR, and nitrogen adsorption/desorption were used to characterize the samples. As a demonstration of potential applications, the thus formed mesoporous anatase TiO_2 nanorods were tested for their photocatalytic efficiency in the degradation of crystal violet, and a photodegradation mechanism is proposed.

S. Priya · J. Robichaud · S. Balaji · Y. Djaoued (✉)
Laboratoire de Micro-spectroscopies Raman et FTIR,
Université de Moncton–Campus de Shippagan,
218, boul. J.-D. Gauthier, Shippagan, NB E8S 1P6, Canada
e-mail: djaoued@umcs.ca

M.-C. Méthot
Institut de recherche sur les zones côtières, 232B Avenue de l'Église, Shippagan, NB E8S 1J2, Canada

J. M. Ehrman
Digital Microscopy Facility, Mount Allison University, 63B York St., Sackville, NB E4L 1G7, Canada

B.-L. Su
Laboratoire de Chimie des Matériaux Inorganiques, The University of Namur (FUNDP), 61 rue de Bruxelles, 5000 Namur, Belgium

Introduction

Due to its physicochemical properties and availability, titanium dioxide (TiO_2) has been the subject of choice for many researchers in the field of solar cells, electrochromic devices, and photocatalysis, just to name a few [1–4]. Hence, great efforts have been directed toward improving the properties of TiO_2 for specific applications by modifying its crystallite structure, particle size, specific surface area, and morphology. For instance, for some photocatalytic applications, nanorods and nanoribbons present significant improvement over fine TiO_2 powders due to their larger specific surface area and the ability to be recovered more easily [5–7]. Until date, several methods such as template technique, replication method, hydrothermal process and soft chemical method have been used for the synthesis of one-dimensional TiO_2 structures. Wang et al. [8, 9] reported the synthesis of one-dimensional titanium glycolate single crystal by the reaction of titanium tetra ethoxide with ethylene glycol in the presence of *n*-butylamine under hydrothermal conditions at 160–170 °C for 5 days and they obtained anatase titania by calcination at 500 °C. Recently, transition metal nanowires were synthesized using ethylene glycol and titanium tetra-*n*-butoxide at 170 °C under atmospheric pressure and anatase titania nanowires were obtained by calcination at 500 °C [10]. Yu et al. [11] prepared titanium glycolate microrods by the mixing of titanium tetra-*n*-butoxide and ethylene glycol at room temperature for 8 h and they observed anatase titania formation at 450–550 °C. All the previously cited works report

a conventional calcination method at high temperature to prepare titania nanorods [5–11].

The improvement of photoactivity of TiO_2 is one of the most important tasks from the point of view of practical use. To achieve this purpose, mesoporous TiO_2 has attracted much attention due to its large surface area and high pore volume [12–14]. However, photocatalytic activities of such materials are limited by the fact that efficient photo-induced charges (electrons and holes) are only generated in materials composed of a well crystallized phase, and preferably in the anatase allotropic form [15]. Usually, the crystallization of amorphous mesoporous TiO_2 requires a calcination at relatively high temperatures (400 °C or above). However, calcination at high temperature may cause the collapse of the framework of mesoporous materials and significantly reduce the specific surface area. Therefore, it is necessary to develop a novel synthetic approach to prepare mesoporous TiO_2 nanorods in the anatase form with high specific surface area.

In the present work, we report on the synthesis of high surface area microporous titanium glycolate nanorods. Subsequently, those as-synthesized nanorods were transformed into anatase TiO_2 mesoporous nanorods by hot water treatment at 90 °C under atmospheric pressure. The microporous to mesoporous transformation proceeds without change in the shape and surface area of the materials. The anatase TiO_2 mesoporous nanorods thus obtained were tested for their application in the photodegradation of crystal violet and compared with tiania nanorods obtained by calcination at 400 °C.

Experimental

Preparation of titanium glycolates and titania nanorods

Following a procedure described by Jiang et al. [10] with modifications, titanium glycolates were synthesized under atmospheric pressure conditions from titanium tetra-etoxide ($(Ti(OEt)_4)$), titanium tetra-isopropoxide ($(Ti(O^iPr)_4)$), and titanium tetra-*n*-butoxide ($(Ti(O^nBu)_4)$). In a typical synthesis, ethylene glycol (40 mL) and the titanium (IV) alkoxide (0.4 mL) were heated with stirring in a reflux system at ~170 °C for 2 h. Afterwards, the solution was cooled to room temperature and the white flocculate that had formed was separated by centrifugation. The white material was washed with de-ionized water and then with ethanol, and dried at 60 °C for 40 min. The as-synthesized titanium glycolates thus obtained all showed a nanorod-like aspect under the optical microscope. Subsequently, the as-synthesized nanorods were treated in hot water at a temperature of <90 °C for 1 h under atmospheric pressure. For comparison, the titanium glycolate nanorods were also calcined at 400 °C. For convenience, we will refer to the titanium glycolate nanorods as TGN.

Characterization

X-ray diffraction (XRD) patterns were obtained from a Philips Analytical PW3710 diffractometer operating at 40 kV and 40 mA and equipped with a Cu cathode (Cu $K_{\alpha 1}$, $\lambda = 1.54056$ Å). The samples in powder form were pressed into a sample holder. The analysis was performed under vacuum at a temperature of 25 °C. High-angle XRD data was run from 5.010 to 79.930° (2θ), with a scan step size of 0.020° (2θ) and a scan step time of 0.5 s. The low-angle XRD was run from 0.5134 to 4.9844° (2θ), with a scan step size of 0.0170° (2θ) and a scan step time of 45.8013 s, using a PW3050/60 goniometer. The particle size Δx was estimated from the Scherrer formula: $\Delta x = 0.9\ \lambda/\Delta 2\theta \cos\theta$, where 2θ is the scattering angle and $\Delta 2\theta$ is the full width at half maximum (FWHM) of a Bragg reflection [16]. The low-angle XRD data of the samples were analyzed by fitting a Gaussian line profile to the curve. The peak values obtained from the fittings were 2.74078 ± 0.00666° (2θ) and 2.27734 ± 0.00746° (2θ). The *d* spacing values of the samples were then obtained from the Bragg reflection formula $2d \sin\theta = n\lambda$. For scanning electron microscopy (SEM) observations, the nanorod samples were dispersed onto 10 mm diameter aluminum stubs covered with double-sided adhesive tape, rimmed with colloidal carbon and coated with ~10 nm gold using a Hummer 6.2 sputtering unit (Anatech Ltd., Hayward, CA). Specimens were examined using a JEOL JSM-5600 SEM (JEOL USA, Peabody, MA) operating at 10 kV and 8 mm working distance. For determination of average length and width of nanorods (or bundles of nanorods), low magnification images (1000–3000×) were overlaid with a 100 pixel grid using Adobe Photoshop CS (Adobe Systems, San Jose, CA). Nanorods or bundles of nanorods that were nearest to a grid intersection, orthogonal to the incident beam and unobscured by other particles were measured. Thirty nanorods from each sample were measured and unpaired *t*-tests assuming unequal variance were used to determine if length and width differed significantly when comparing each sample treatment to the original prepared material. High magnification images (30000×) were collected to examine changes to the surface of nanorods with treatment. Transmission electron microscopy (TEM) of the nanorods was performed by placing a small amount of the samples into a glass vial. Ethanol was added and the solution was sonicated for 10 min. A drop of the solution was placed onto a carbon coated 200 mesh copper grid and left to dry overnight. The sample was imaged using a 2011 JEOL STEM at 200 keV. Images were captured on a 4k × 4k multiscan CCD camera using Digital Micrograph from

Gatan. Solid state NMR experiments were carried out on a Bruker Avance NMR spectrometer with a 9.4T magnet (400 MHz proton Larmor frequency, 100.65 MHz ^{13}C Larmor frequency) using double resonance HX probe head for rotors of 4 mm diameter. The samples were spun at 12 kHz for the proton spectra and 7 (or 8 kHz) for the ^{13}C MAS spectra to determine center bands and to identify possible spinning sidebands. For the ^{13}C MAS NMR spectrum between 1024 and 1096 scans were accumulated, using 500 μs CP contact times. Nitrogen adsorption and desorption isotherms for the as-synthesized samples were obtained on a Micromeritics ASAP 2010 system at liquid nitrogen temperature. The samples were degassed at 80 °C overnight before measurements were made. The specific surface area was determined by the Brunauer–Emmett–Teller (BET) method and the pore size distribution was obtained from the Horvath–Kawazoe (HK) model. For the hot water treated and calcined samples, the nitrogen adsorption and desorption isotherms were obtained on a Micromeritics Tristar 3000 system. The specific surface area was determined by the BET method and the pore size distribution was obtained from the N_2 adsorption branch of the isotherm using the Barett–Joyner–Halenda (BJH) method. Raman spectra were recorded at room temperature with a Jobin-Yvon Labram HR microanalytical spectrometer. The spectra were generated with a 17 mW, 632.8 nm, He–Ne laser excitation and were dispersed with the 1800 g/mm grating across the 0.8 m length of the spectrograph. The spectral resolution of this apparatus is estimated to be less than 0.5 cm^{-1} for a slit width of 150 μm and a confocal hole of 300 μm. The photocatalytic activity of titania nanorods prepared using the $Ti(O^nBu)_4$ precursor was quantified by monitoring the degradation of crystal violet (CV) with UVC ($\lambda = 200$–290 nm) irradiation. The initial concentration of the dye was 20 mg/L in de-ionized water. The laser power was 9 mW on the sample surface. UV irradiation of CV was performed using a Luzchem irradiation chamber of 32 cm (W) × 33 cm (D) × 21 cm (H) equipped with six top, four left side and four right side UVC lamps. The photo reactivity experiment was carried out in a quartz container of about 80 mL capacity. In a typical procedure, 60 mL of crystal violet solution was taken with 50 mg of titania nanorod powder and the suspension was premixed in the dark for 30 min to establish the adsorption/desorption equilibrium of crystal violet on the photocatalytic surface. Aliquots (3 mL) were collected periodically from the reactor during illumination. The samples were taken from the photo reactor at 0, 2, 4, 6, 8, 10, 20, 30, 40, 50, 60 and 120 min. To settle the catalyst the solution was centrifuged at 8000 rpm for 10 min and the supernatant was analyzed by UV–Vis spectrophotometry in the range 200–1000 nm (Biochrome Ultraspec 2000) using a quartz cell. In order to verify the self-photolysis of CV, a blank test was also carried out by irradiating the CV homogeneous solution without the TiO_2 photocatalyst. The adsorption of the dye on the surface of the photo catalyst was investigated by stirring the aqueous solution (60 mL) in the dark for several hours with 50 mg of photocatalyst. Analysis of the sample after centrifugation indicates some observable adsorption of the dye on the surface of the catalyst, but it remains the same after 30 min. The degradation of crystal violet was ascertained from the follow up of the absorption peak at 519 nm.

Results and discussion

SEM and TEM studies

SEM study was conducted to reveal the nanorod features of the synthesized products. A closer examination indicates that some of the nanorods might have aggregated into bundles and thus appeared thicker than expected when viewed under SEM at low magnification. The three types of as-synthesized TGN specimens prepared from $Ti(OEt)_4$, $Ti(O^iPr)_4$, and $Ti(O^nBu)_4$ varied considerably in length and width (Table 1, Fig. 1a, d, and g). TGN prepared from $Ti(O^nBu)_4$ were the longest and widest, while those prepared from $Ti(O^iPr)_4$ were the shortest and narrowest.

The hot water treatment at 90 °C (Fig. 1b, e, and h) and the calcinations at 400 °C (Fig. 1c, f, and i) generally shortened the nanorods and made individual particles narrower. Shortening of nanorods appeared to result from simple breakage of longer rods, while narrowing apparently resulted from the separation of bundles of smaller nanorods adhering to each other. However, there were exceptions to this general observation. Calcination of TGN prepared from $Ti(O^nBu)_4$ did not produce a statistically significant narrowing, and those prepared from $Ti(O^iPr)_4$ were not significantly affected in either dimension by the same treatment (Table 1). Calcinations at 400 °C also induced a visible bending or curling to some of the nanorods of all types (Fig. 1c, f, and i).

Both the hot water treatment at 90 °C and calcinations at 400 °C changed the surface characteristics of most nanorod types, with the exception of calcinations of the TGN prepared from $Ti(O^iPr)_4$. For all the other rod types, hot water treatment and calcination produced a roughening of the surface, both in the form of fine blebbing and the appearance of larger particles, presumably small pieces of broken rod (Fig. 2a–h). Heat treatment of the TGN prepared from $Ti(O^iPr)_4$ did not visibly alter the surface (Fig. 2i).

Figures 3a–i and 4a–i show the TEM images of the same samples as in Fig. 1a–i. A close examination of the TEM images show clearly that the nanorods are constituted of an

Table 1 Mean length and width of 30 nanorods (or bundles) from each sample and treatment

Sample	Length (μm) [SD]	Treatment effect [*p*]	Width (μm) [SD]	Treatment effect [*p*]
As-synthesized from $Ti(O^nBu)_4$	17.63 [6.54]		1.85 [0.73]	
Hot water treated	9.40 [5.41]	Yes [<0.001]	1.36 [0.69]	Yes [0.005]
Calcined	11.46 [8.63]	Yes [0.002]	1.51 [1.05]	No [0.074]
As-synthesized from $Ti(OEt)_4$	6.22 [3.34]		0.97 [0.29]	
Hot water treated	3.71 [3.13]	Yes [0.002]	0.69 [0.26]	Yes [<0.001]
Calcined	2.99 [2.37]	Yes [<0.001]	0.46 [0.17]	Yes [<0.001]
As-synthesized from $Ti(O^iPr)_4$	5.67 [3.23]		0.63 [0.26]	
Hot water treated	3.42 [2.57]	Yes [0.002]	0.50 [0.32]	Yes [0.041]
Calcined	5.11 [3.80]	No [0.269]	0.69 [0.40]	No [0.271]

Standard deviation for length and width are given in brackets. The results of paired *t*-tests for treatment effect on length and width are given in adjacent column with the *p* value indicated in brackets

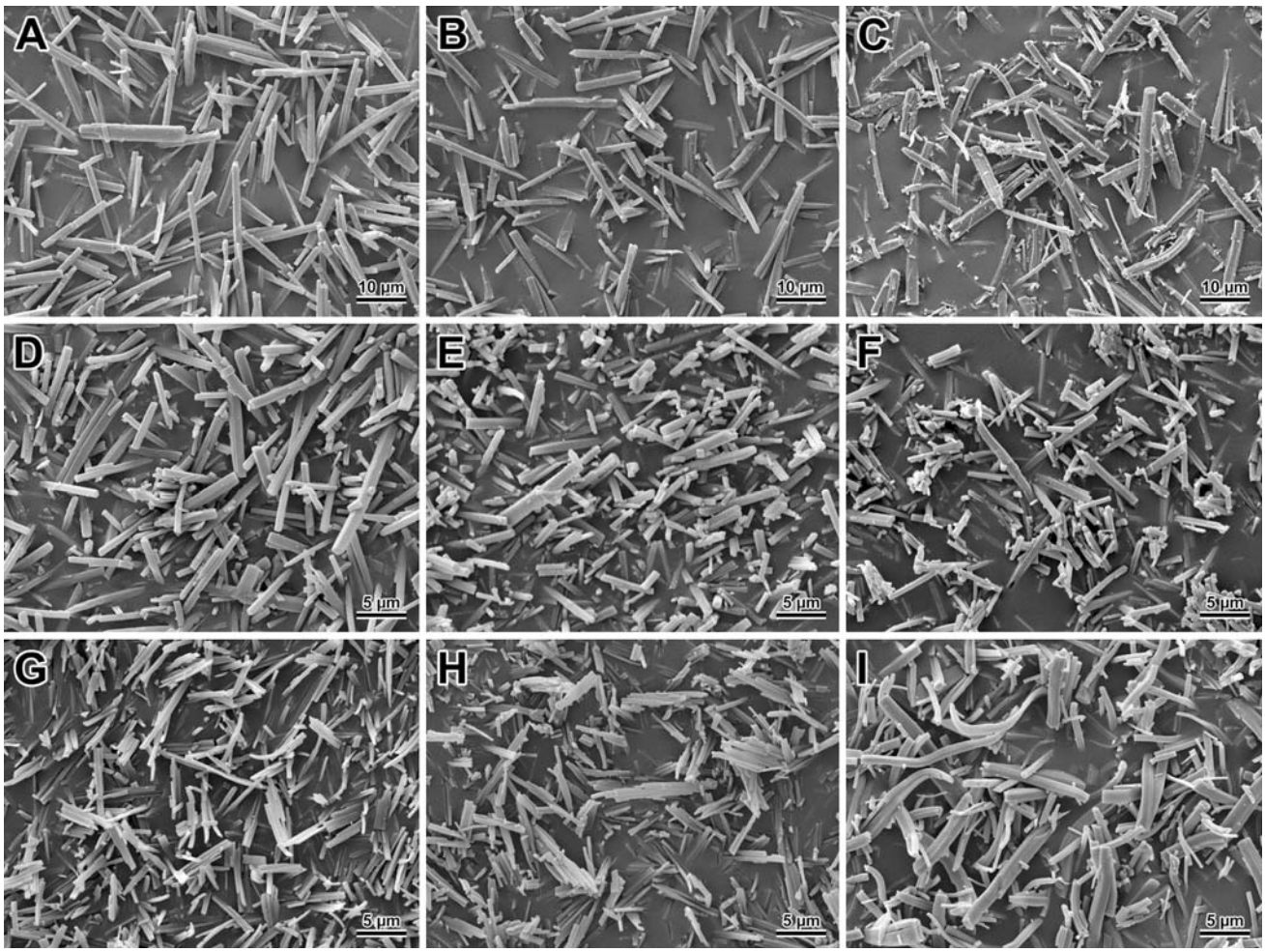

Fig. 1 Low magnification SEM images of TNG: from $Ti(O^nBu)_4$ **a** as-synthesized, **b** hot water treated, **c** calcined at 400 °C; from $Ti(OEt)_4$ **d** as-synthesized, **e** hot water treated, **f** calcined at 400 °C; from $Ti(O^iPr)_4$ **g** as-synthesized, **h** hot water treated, **i** calcined at 400 °C. Note the tendency of nanorods to bend or curl with 400 °C heating

agglomeration of nanometer-sized particles. The TEM images confirm that the morphology is preserved during the process of hot water treatment or calcination. The TEM images show the formation of mesopores with a disordered wormhole-like array following the hot water treatment or calcination.

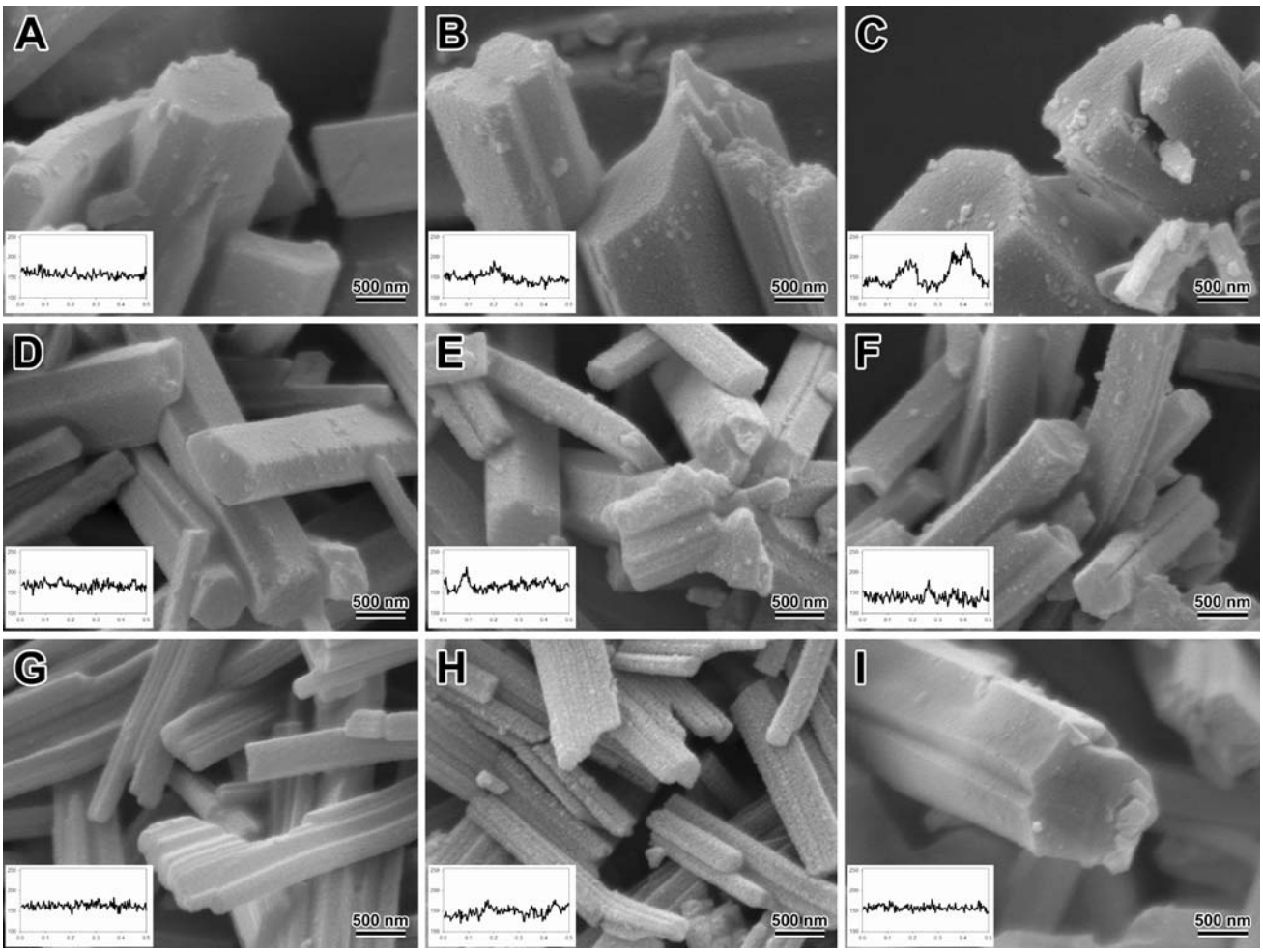

Fig. 2 High magnification SEM images of TGN: from $Ti(O^nBu)_4$ **a** as-synthesized, **b** hot water treated, **c** calcined at 400 °C; from $Ti(OEt)_4$ **d** as-synthesized, **e** hot water treated, **f** calcined at 400 °C; from $Ti(O^iPr)_4$ **g** as-synthesized, **h** hot water treated, **i** calcined at 400 °C. The images show changes to surface roughness of rods with treatments. Inset is a graph of gray-scale values from a 500 nm transect along the outside of a rod, parallel to the long axis. SEM level and gain remained constant through image collection, but these results are only indicative of changes in roughness and should not be considered quantitative

μ-Raman studies

Figure 5a shows the Raman spectrum of the as-synthesized TGN prepared from $Ti(O^nBu)_4$. It displays sharp bands owing to its crystalline nature. The bands at 606.2 and 644.1 cm^{-1} are assigned to Ti–O stretching vibration. The Ti–O–C stretching bands characteristic of ethylene glycolate ligands linked to titanium appear at 1033, 1091 and 1116 cm^{-1}. The spectral pattern of the as-synthesized TGN changed entirely after the hot water treatment at ~90 °C for 1 h (Fig. 5b). The bands corresponding to ethylene glycolate ligands linked to titanium disappeared, indicating that the organic molecules leached out of the nanorods. The removal of ethylene glycol template was evidenced by the Raman analysis of the filtrate recuperated after the hot water treatment of the as-synthesized TGN. The Raman spectrum of the resultant product is shown in Fig. 5b which shows the Raman modes at 151.8, 406.0, 517.5, and 636.7 cm^{-1}. These bands are characteristic features of nanocrystalline TiO_2 in the anatase form [17]. The anatase main band is very broadened (FWHM = 22.0 cm^{-1}) and high-frequency shifted (151.8 cm^{-1}) with respect to the values of commercial anatase TiO_2 powder (7.5 and 142.5 cm^{-1}), indicating that the nanorods are constituted of titania nanoparticles [15]. A phonon confinement study performed on the TiO_2 nanorods obtained after hot water treatment shows that the observed shift and broadening correspond to a particle size of ~5 nm [18]. This result is in agreement with the TEM morphology which shows that the TiO_2 nanorods obtained after hot water treatment are formed of nanoparticles. Figure 5c shows the Raman spectrum of the as-synthesized TGN calcined at 400 °C for 1 h. It can be seen from the spectrum that the crystallization to anatase was complete as evidenced from the characteristic

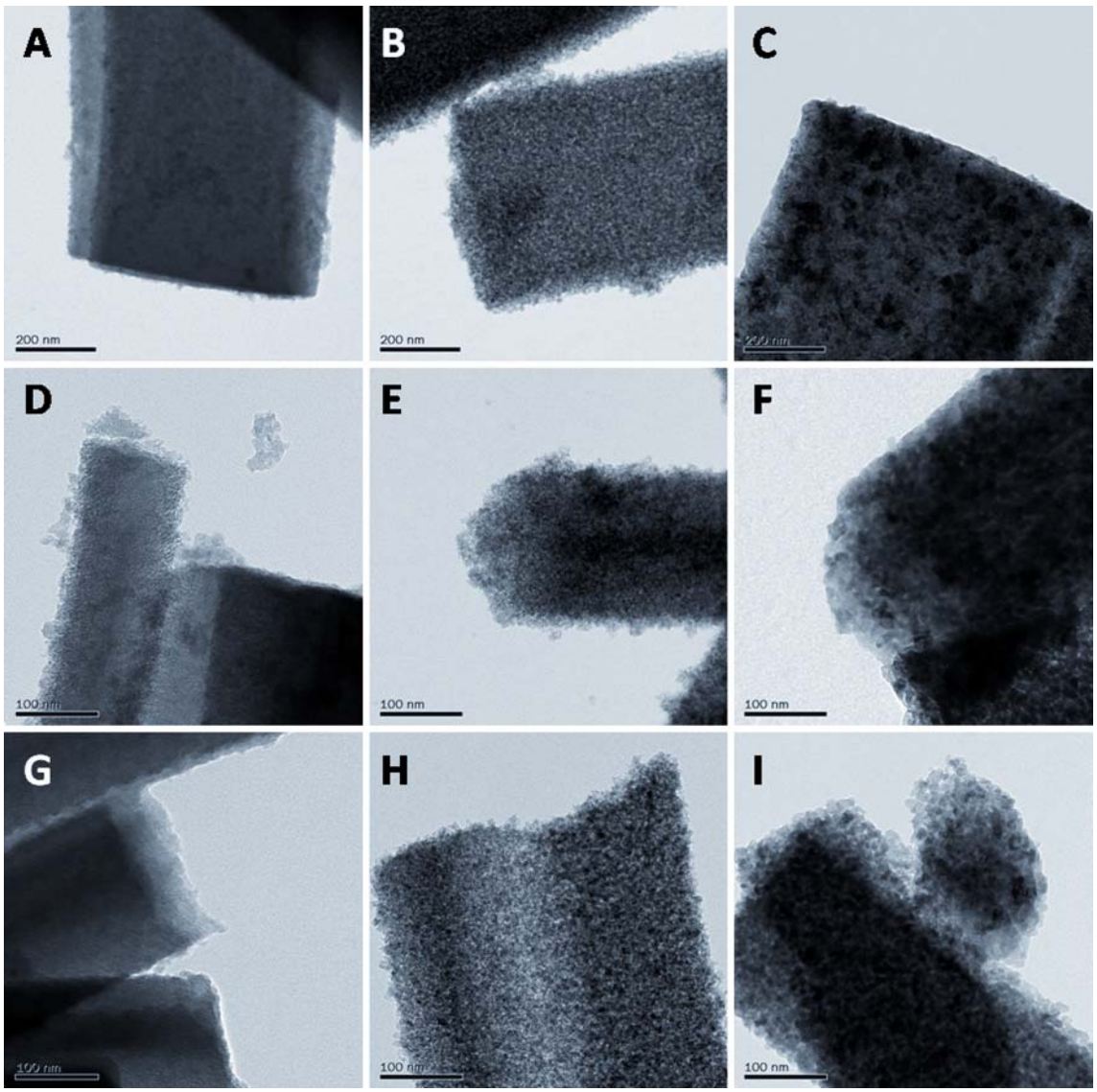

Fig. 3 TEM images of TNG: from $Ti(O^nBu)_4$ **a** as-synthesized, **b** hot water treated, **c** calcined at 400 °C; from $Ti(OEt)_4$ **d** as-synthesized, **e** hot water treated, **f** calcined at 400 °C; from $Ti(O^iPr)_4$ **g** as-synthesized, **h** hot water treated, **i** calcined at 400 °C

anatase Raman modes at 145.1, 197.8, 396.4, 514.6, and 638.6 cm^{-1} when the as-synthesized TGN were annealed at 400 °C. The main anatase Raman band is centered at 145.1 cm^{-1} with a FWHM of 12.3 cm^{-1}, corresponding to a crystallite size of $\sim$11 nm as per the phonon confinement study. A comparison of obtained Raman data on anatase TiO_2 has been made with the values obtained by Ohsaka et al. [19]. They studied the single crystal of TiO_2 both natural and synthetic types. In that study, the scattered light was collected at 90° to the incident light. The α_{xx} spectrum exhibits two peaks at 516 and 399 cm^{-1} with a weak mode at 144 cm^{-1}, whereas α_{xz} spectrum exhibits three strong modes at 144, 197 and 639 cm^{-1} (see Table 2) [19]. In comparison to Ohsaka's work, we can note that the Raman modes in our samples show considerable shift in the peak position. As mentioned above, the obtained shifts are attributed to the confinement of phonons in the nanoparticles of TiO_2 that constitute the synthesized nanorods. The Raman spectra of the nanorods prepared from $Ti(OEt)_4$, and $Ti(O^iPr)_4$ look similar to the ones shown in Fig. 5.

X-ray diffraction (XRD) studies

Figure 6 shows the wide- and low-angle XRD patterns of the as-synthesized, hot water treated and calcined TGN prepared from $Ti(OEt)_4$. The wide- and low-angle XRD patterns of the nanorods prepared from $Ti(O^iPr)_4$ and $Ti(O^nBu)_4$ look similar to the ones shown in Fig. 6. As seen in Fig. 6a, the as-synthesized TGN sample exhibit diffraction lines assignable to crystalline titanium glycolate. After hot water treatment at

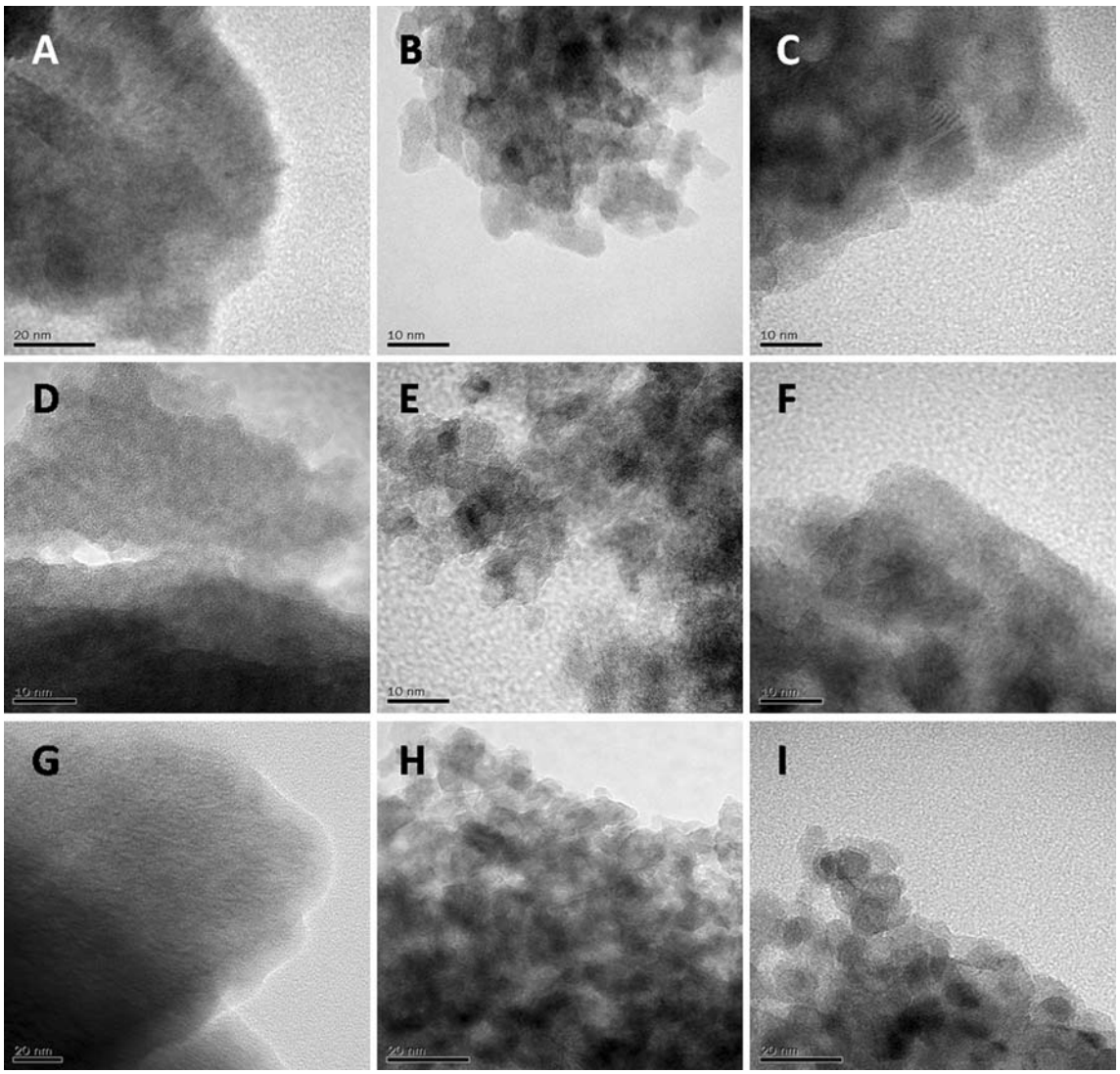

Fig. 4 High resolution TEM images of TNG: from $Ti(O^nBu)_4$ **a** as-synthesized, **b** hot water treated, **c** calcined at 400 °C; from $Ti(OEt)_4$ **d** as-synthesized, **e** hot water treated, **f** calcined at 400 °C; from $Ti(O^iPr)_4$ **g** as-synthesized, **h** hot water treated, **i** calcined at 400 °C

90 °C for 1 h under atmospheric pressure, the as-synthesized TGN transformed to anatase TiO_2 (JCPDS card no: 21-1272) (Fig. 6b). The broad diffraction peaks indicate that the samples are composed of small crystallites with a size of nanometer scale.

When calcined at 400 °C, the as-synthesized TGN also transformed to anatase (Fig. 6c). The peaks were rather sharp, which indicated relatively high crystallinity. After treatment in hot water at 90 °C, the crystallite size is ~3.9 nm. Upon annealing at 400 °C, the crystallite size increases to ~13.3 nm. The hot water treated TGN samples prepared from $Ti(O^iPr)_4$ and $Ti(O^nBu)_4$ exhibited a crystallite size of 4.6 and 5 nm, respectively. After calcination at 400 °C, the crystallite sizes increased to 19 and 20.5 nm, respectively. Furthermore, the crystallite sizes as calculated from XRD increase as the molecular weight of the precursor used in the samples preparation increases. The low-angle diffraction patterns of the as-synthesized TGN show two diffraction peaks, one well-defined with lattice spacing $d = 115.96$ Å and one broad with $d = 32.208$ Å (insets to Fig. 6a, b).Whereas the hot water treated TGN shows two peaks at $d = 115.96$ Å and one broad with $d = 38.76$ Å. After calcination at 400 °C, only one diffraction peak appears with $d = 115.87$ Å (inset Fig. 6c). There is almost no shift of the diffraction peak with $d \sim 116$ Å exhibited by the low-angle diffraction patterns of the hot water treated and calcined nanorod samples, compared to the as-synthesized product. The origin of the peak with $d \sim 116$ Å could not be identified, it may be attributed to the beam effect.

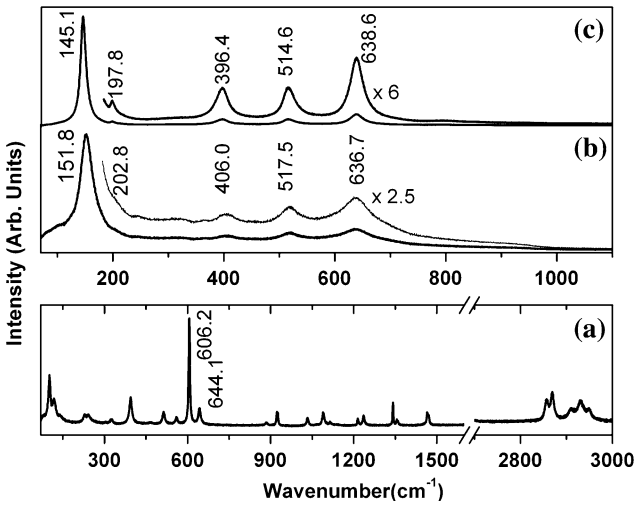

Fig. 5 Raman spectra of the TGN prepared from $Ti(O^nBu)_4$ **a** as-synthesized, **b** hot water treated, **c** calcined at 400 °C

NMR studies

Figure 7 shows the comparison of ^1H MAS NMR spectra of the as-synthesized (a), hot water treated (b), and calcined (c) TGN prepared from $Ti(O^nBu)_4$. From the spectra of as-synthesized TGN, it is seen that the CH_2 protons of glycolate are equivalent and they resonate at around 3.5 ppm. A broad peak around 5.5 ppm could be assigned to OH group of ethylene glycol. In addition, the spectrum of titanium glycolate nanorods has a peak at 0.89 ppm, which could be due to CH_3 group of ethanol (the CH_2 group of ethanol merges with CH_2 of as-synthesized TGN). The adsorbed ethanol was not seen when deuterated ethanol was used for washing instead of ethanol. This is in good agreement with XRD and Raman spectroscopic data. The ^1H MAS NMR spectra of titania nanorods obtained from calcination (b) and the one obtained from hot water treatment (c) have only one peak due to –OH group at 5.5 and 5.9 ppm, respectively. This further confirms the complete removal of the ethylene glycol template from the nanorods.

The ^{13}C MAS NMR spectra of as-synthesized TGN (figure not shown here) exhibit two well-resolved peaks around 63.7 and 75.1 ppm, due to CH_2 groups of ethylene glycol, which are bonded through covalent and coordinate bonds. The carbon atoms of free ethylene glycol and those bonded to oxygen in other polymeric species have the chemical shift values around the range 60–65 ppm. [20, 21]. We observed no peak in the ^{13}C NMR data of the TGN sample heated to 400 °C, as it is completely converted to titania. Similarly, the nanorods obtained by hot water treatment do not have any peak in the ^{13}C MAS NMR spectrum owing to the absence of carbon content in the sample.

Textural properties

The N_2 adsorption-desorption isotherms of the as-synthesized, hot water treated and calcined TGN prepared from

Table 2 Raman active modes of hot water treated and calcined TGN as compared to the Raman modes observed in natural and synthetic anatase crystals reported by Ohsaka et al.

Raman active modes	Peak positions from Ohsaka et al. (cm^{-1})	Peak positions for hot water treated TGN (cm^{-1})	Peak positions for calcined TGN (cm^{-1})
Eg(1)	144	151.8	145.1
Eg(2)	197	202.8	197.8
B1g(1)	399	406.0	396.4
B1g(2)	519	517.5	514.6
A1g	513		
Eg(3)	639	636.7	638.6

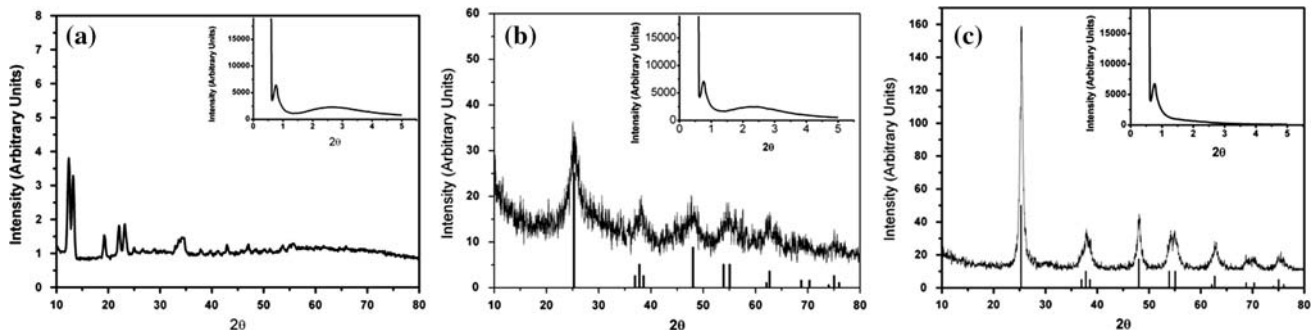

Fig. 6 Wide- and low-angle (*inset*) XRD patterns of the TGN prepared from $Ti(OEt)_4$ **a** as-synthesized, **b** hot water treated, **c** calcined at 400 °C

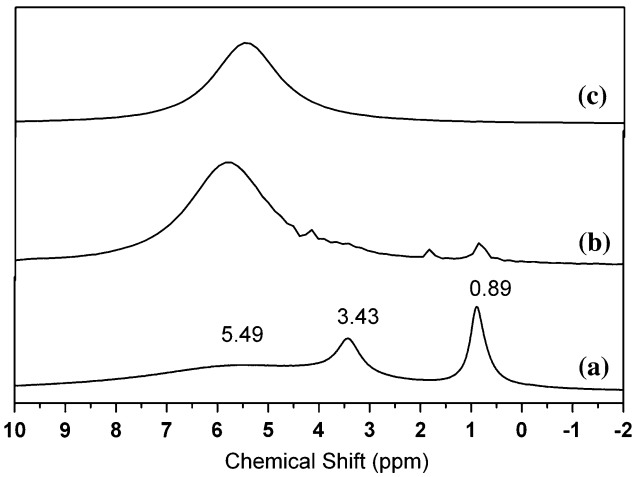

Fig. 7 ^{1}H MAS NMR spectra of TGN (a) as-synthesized, (b) hot water treated, and (c) calcined at 400 °C

$Ti(OEt)_4$ are shown in Fig. 8. For the samples prepared from $Ti(O^iPr)_4$ and $Ti(O^nBu)_4$, the isotherms look similar to the ones shown in Fig. 8. The as-synthesized TGN exhibit microporous features as confirmed by type I N_2 adsorption-desorption isotherms (Fig. 8a). A very high surface area (480 m^2/g) is obtained, and the pore size distribution is centered in the microporous range (1.1 nm). The pore volume, as determined by the HK method, is 0.26 cm^3/g. The corresponding results obtained for the TGN prepared from the $Ti(O^iPr)_4$ precursor are 437 m^2/g and 0.27 cm^3/g, respectively. This is the first report regarding the textural properties of as-synthesized nanorods. Figure 8b shows the N_2 adsorption-desorption isotherms and the corresponding BJH pore size distribution curves (inset) of the TGN after hot water treatment at 90 °C for 1 h. The adsorption-desorption isotherms are type IV, characteristic of a mesoporous compound. This result is interesting as it shows that microporous titanium glycolate transformed into mesoporous anatase TiO_2 nanorods. The surface area remains almost unchanged (477 m^2/g), and the pore volume and pore size become larger (1.6 cm^3/g and 3 nm, respectively), indicating that the ethylene glycolate ligands linked to titanium present in the as-synthesized TGN have been leached out by hot water treatment. When the as-synthesized microporous TGN were calcined at 400 °C (Fig. 8c), they also transformed into mesoporous anatase TiO_2 nanorods but with a large decrease in the surface area (155 m^2/g), while the pore sizes increased with the calcination temperature. In fact, because of the increased crystallization during calcination, the growth of nanoparticles occurs, and the interspaces between the particles will be enlarged, leading to the enlargement of the mesopore size. The textural properties of the nanorods prepared from $Ti(OEt)_4$, $Ti(O^iPr)_4$ and $Ti(O^nBu)_4$ are provided in Table 3. The retention of high surface areas is seen during the conversion of microporous TGN to mesoporous anatase nanorods by hot water treatment at 90 °C. It is particularly noteworthy that the mesostructured anatase nanorods reported in Table 2 have BET surface areas substantially larger than those of mesostructured one-dimensional TiO_2 materials previously reported. Zhang and Qi [22] obtained mesoporous anatase titania nanowires with BET specific surface area of 61 m^2/g after calcinations at 500 °C to remove the template which consisted of bacterial cellulose membranes. Chae et al. reported the fabrication of mesoporous titania nanofibers by using a triblock copolymer template within a porous alumina template. The triblock copolymer and the porous alumina were removed by calcination and dissolution, respectively. The BET specific surface area of the resulting anatase titania nanofibers was found to be 34.9 m^2/g [23]. Yu et al. have prepared mesoporous titania nanorod/titanate nanotube composites by using TiF_4 and H_3BO_3 as precursors. They found a specific surface area of 225.4 m^2/g for the obtained composites [24]. Thus, the BET surface areas found in this work for the mesoporous anatase TiO_2 nanorods obtained by hot water treatment at 90 °C are much higher than the values reported in the literature.

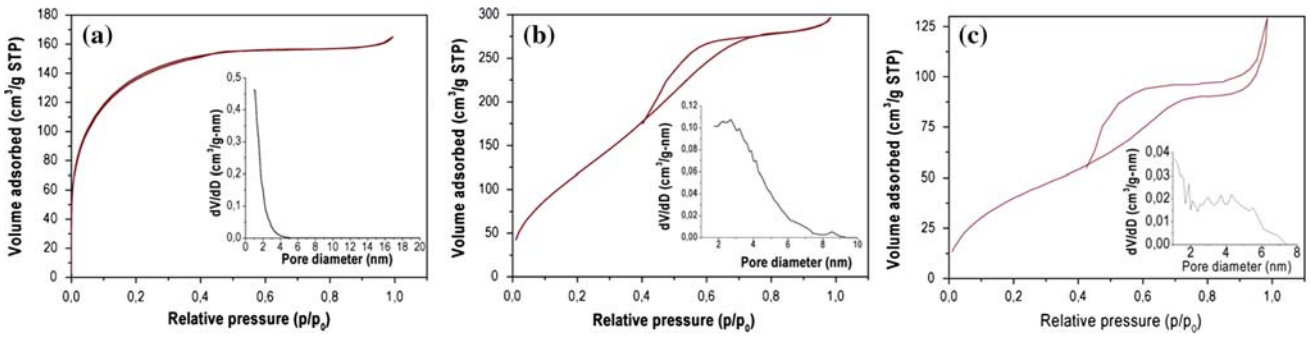

Fig. 8 N_2 adsorption-desorption isotherms and corresponding pore size distribution curves (*inset*) of the TGN prepared from $Ti(OEt)_4$ **a** as-synthesized, **b** hot water treated, **c** calcined at 400 °C

Table 3 Textural properties of the as-synthesized, hot water treated, and calcined nanorods

Sample	S_{BET} (m^2/g)	Pore volume (cm^3/g)	Pore diameter (nm)
As-synthesized from $Ti(OEt)_4$	480	0.26	1.1[a]
Hot water treated	477	1.6	2.2[b]
Calcined	156	1.3	3.8[b]
As-synthesized from $Ti(O^iPr)_4$	437	0.27	1.6[a]
Hot water treated	418	1.6	2.2[b]
Calcined	85	0.44	3.8[b]
As-synthesized from $Ti(O^nBu)_4$	ND	ND	ND
Hot water treated	499	1.1	2.6[b]
Calcined	65	0.31	3.9[b]

[a] Median pore diameter obtained from the HK method

[b] Average pore diameter obtained from the BJH method

Mechanism of the transformation of microporous TGN into mesoporous anatase TiO_2 nanorods

The X-ray structure of titanium glycolate single crystal [$Ti(OCH_2CH_2O)_2$] synthesized by the reaction of Ti(O^nBu)$_4$ with ethylene glycol in the presence of *n*-butylamine under hydrothermal conditions at 160–170 °C for 5 days was reported by Wang et al. [25]. The staggered arrangement of Ti–O skeleton in titanium glycolate single crystal is similar to that of the TiO_2 anatase structure. In as-synthesized TGN obtained from ethylene glycol and $Ti(OEt)_4$, or $Ti(O^iPr)_4$, or $Ti(O^nBu)_4$, ethylene glycol bridges adjacent titanium centers and it forms a chelate with titanium metal centers. It is depicted in Scheme 1. Thus, the mode of binding of ethylene glycol has a staggered Ti–O skeleton and results in a polymer network. Upon hot water treatment, the as-synthesized TGN undergoes hydrolysis to give Ti–OH bond with the expulsion of ethylene glycol and ROH (R = Et, nBu, ^{i}Pr). Furthermore, the expulsion of ethylene glycol was evidenced by Raman in the hot water recuperated after treatment of the as-synthesized TGN. The absence of ethylene glycol and ROH is also confirmed by the solid state ^{1}H MAS NMR (see Fig. 7) and ^{13}C MAS NMR data. This expulsion of ethylene glycol by hot water treatment might possibly lead to the formation of the mesoporous structure. During the hydrolysis reaction, the Ti–O skeleton remains intact. This step is shown in Scheme 2. The Ti–OH bonds undergo condensation with neighboring Ti–OH forming Ti–O–Ti three-dimensional networks leading to the formation of anatase TiO_2. The Raman spectrum of the hot water treated TGN sample shows that it is anatase TiO_2-nanorods (see Fig. 5). This is further confirmed by XRD data (see Fig. 6). The whole process of forming the TiO_2 network is shown in Scheme 3. Recently, Gröhn et al. [26] reported that the polymers dispersed in dendrimers were used as a template-matrix for the formation of inorganic nanoclusters. The nanoclusters formed inside the polymer-dendrimer network are stabilized by the polymer-dendrimer matrix. In titanium glycolate polymer, the Ti–O backbone is stabilized by the polymeric network containing the titanium glycolate molecules. Thus, the polymer chain containing Ti–O in the backbone results in clusters of nanometer size and forms smaller TiO_2 particles.

Photocatalytic activity

The absorption spectrum of CV is characterized by three bands in the UV region. Two bands at 208 and 249 nm,

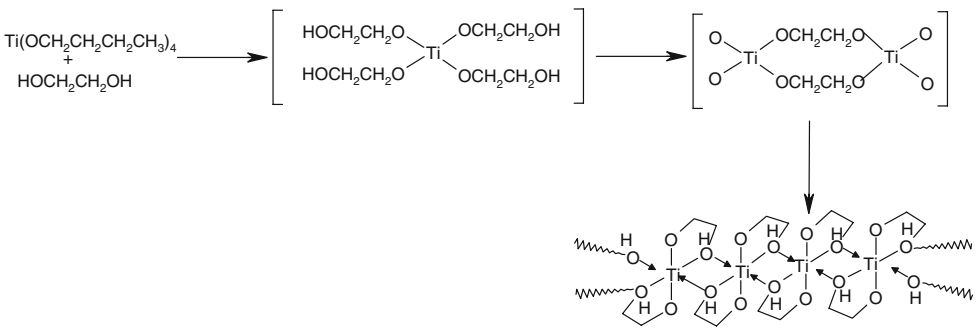

Scheme 1 Reaction of Ti(O^nBu)$_4$ with ethylene glycol resulting in titanium glycolate nanorods. The scheme shows the mode of binding of ethylene glycol with the titanium centers in the compound

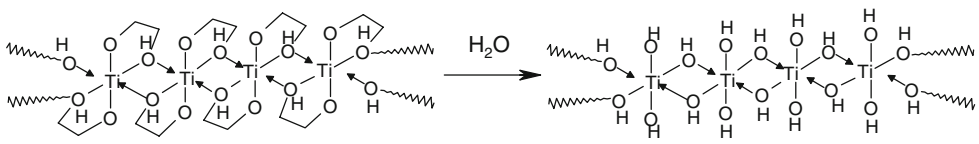

Scheme 2 Upon hot water treatment, hydrolysis titanium glycolate nanorods undergoes hydrolysis to give Ti–OH bond with the expulsion of ethylene glycol and ROH (R = Et, nBu, ^{i}Pr)

Scheme 3 Condensation of the Ti–OH bonds with neighboring Ti–OH forming Ti–O–Ti three dimensional networks leading to the formation of anatase TiO_2 nanorods

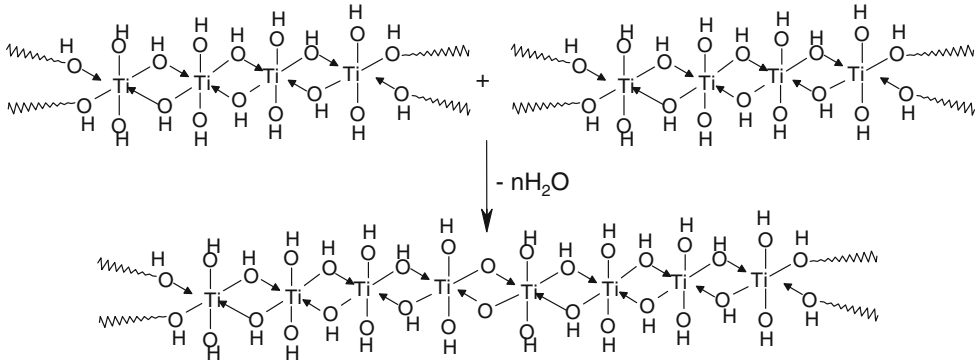

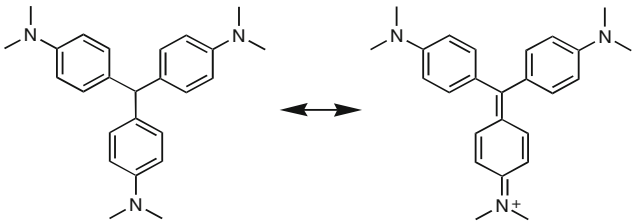

Scheme 4 The quinoidal form of crystal violet structure

corresponding to $\pi \rightarrow \pi^*$ transitions of the aromatic rings, and a band at 303 nm is due to $n \rightarrow \pi^*$ transition. A band in the visible region located at 591 nm is due to $\pi \rightarrow \pi^*$ transition arising from quinoidal form of CV, where all three terminal amino groups are in the resonance system by conjugation. The quinoidal form of crystal violet structure is shown in Scheme 4.

The degradation of CV was accessed by the follow up of the absorbance changes at 591 nm by UV–Vis spectrometry. The absorption spectral changes during photodegradation of CV in aqueous solution by titania nanorods obtained from hot water treatment as well as by those obtained from calcination at 400 °C are shown in Fig. 9. With increasing irradiation time, the absorbance of the peak at 591 nm decreased, with a shift in the absorption wavelength from 591 to 560 nm and the color of the CV solution changed from violet to pink. This color change and the shift in the wavelength could be due to *N*-demethylation process [25]. The residual concentration of CV as a function of irradiation time in aqueous solutions is shown in Fig. 10. It is observed that the concentration of residual CV decreases exponentially with time and almost disappears at 60 min in the presence of both titania nanorod samples (hot water treated and calcined), resulting in complete decolorization of the solution. Calcined TiO_2 nanorods degraded about 2.5 ppm CV (12.5% of the initial concentration) within 10 min, while hot water treated titania nanorods degraded about 12.4 ppm CV (62% of the initial concentration) during the same time period. Complete decolorization of the CV solution was observed in ~50 min with hot water treated samples, while for calcined samples it took around 60 min. When CV dye is exposed to UVC alone (i.e. in the absence of TiO_2 nanorods) only 1.6 ppm CV (8% of the initial concentration)

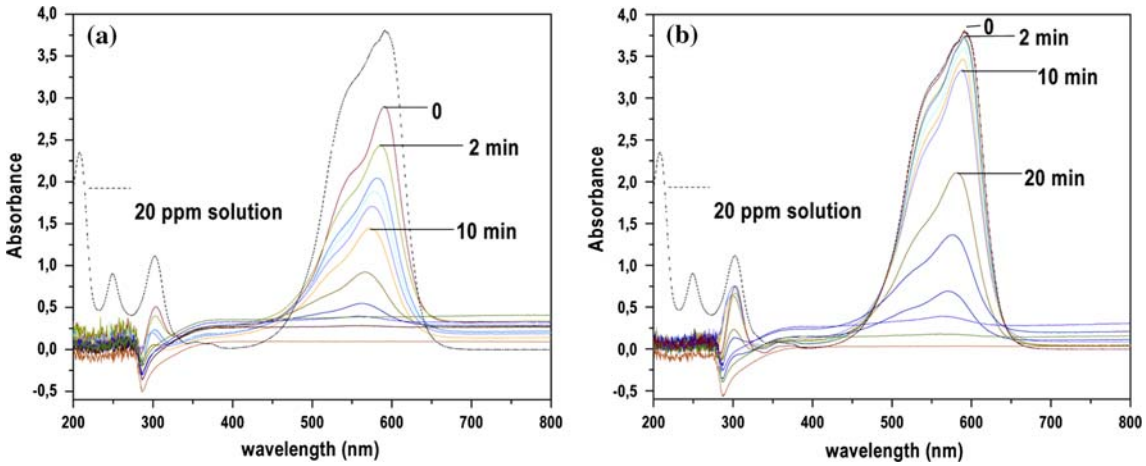

Fig. 9 UV–Vis spectral changes of crystal violet in aqueous solution as it degrades with time under the action of mesoporous TiO_2 nanorod photocatalysts prepared **a** by hot water treated, **b** calcined at 400 °C when irradiated with UVC (~250 nm) light

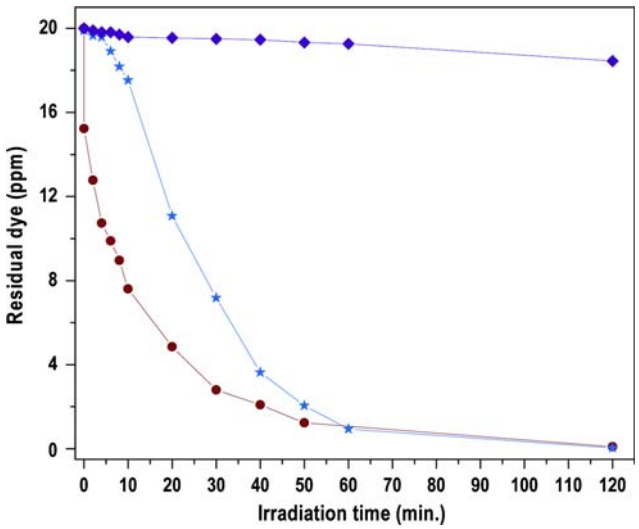

Fig. 10 Degradation profiles of crystal violet with time, when exposed to UVC alone (*diamond*), UVC + mesoporous TiO_2 nanorods prepared by hot water treatment (*dot*), and UVC + mesoporous TiO_2 nanorods calcined at 400 °C (*star*)

was degraded after 2 h (see Fig. 10, diamond). The higher photocatalytic efficiency of the hot water treated TiO_2 nanorods is principally attributed to its enhanced surface area as observed from the BET measurements. These mesoporous anatase TiO_2 nanorods obtained after hot water treatment were reused as photocatalyst without any further treatment, and their efficiency remains the same when recycled.

Photodegradation mechanism of crystal violet

As seen in Scheme 5, there are two competitive mechanisms involved in the photodegradation of CV. One mechanism involves de-methylation while the aromatic structure of CV is preserved. The other pathway involves the destruction of the aromatic conjugative structure, which results in instant bleaching [27]. In the first process, the active oxygen generated on the surface of TiO_2 nanoparticles due to UV irradiation attacks the N atom of CV, and it results in the demthylation at N center. Chen et al. have reported recently the photodegradation of crystal violet on TiO_2. They have identified the intermediates formed during each step of the photodegradation by using UV–Vis and HPLC with a photodiode array detector and ESI mass spectrometry. The hypsochromic shift of the UV–Vis absorption they observed from 588.3 to 543.2 nm was attributed to the formation of series of *N*-demethylated intermediates in a stepwise manner.

Similarly, we have also observed hypsochromic shift of the peak absorption from 591.5 to 563 nm stepwise. This hypsochromic shift is due to consecutive *N*-demethylation reactions, corresponding to removal of two, three and four methyl groups. The formation of intermediates due to photodegradation is shown in Scheme 5. Crystal violet on reaction with active oxygen forms $CV^{+\bullet}$ radical. This radical further degrades by the action of $O_2^{\bullet}$ or $OH^{\bullet}$ to form series of *N*-demethylated products. First it forms intermediate **A** *N*,*N*-dimethyl, *N*′*N*′-dimethyl, *N*′′-methyl

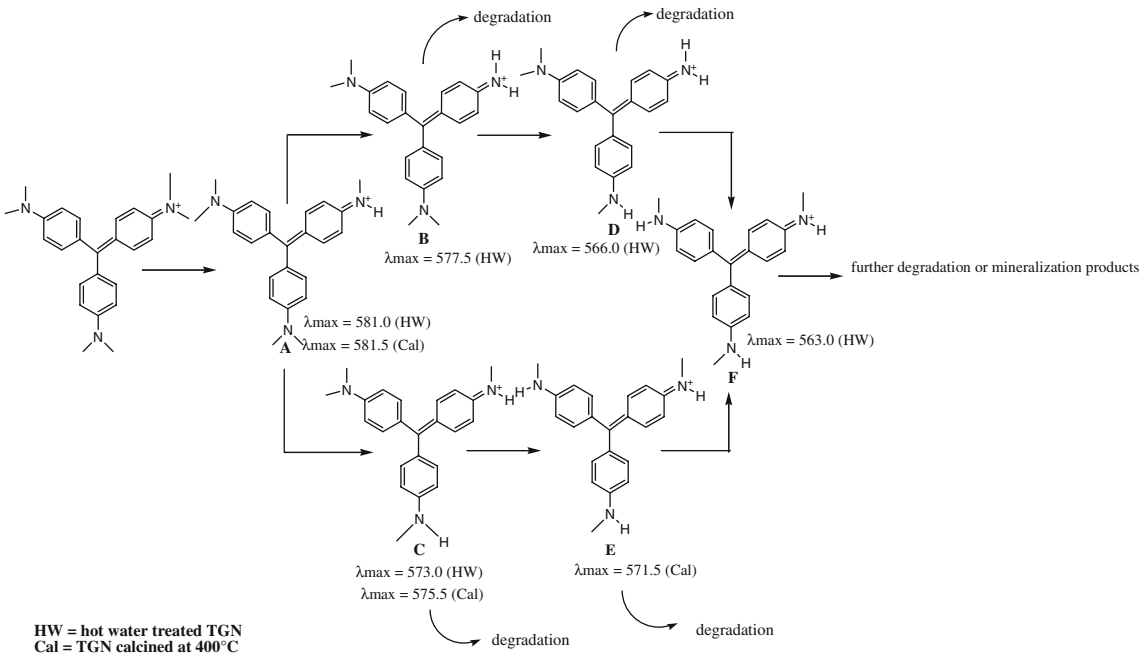

Scheme 5 Mechanisms involved in the photodegradation of crystal violet

pararosaniline ($\lambda_{max} = 581.0$ nm). Intermediate **A** undergoes further degradation to form di-*N*-demthylated intermediates **B** *N*,*N*-dimethyl, *N*′*N*′-dimethyl pararosaniline ($\lambda_{max} = 579.8$ nm) and **C** *N*,*N*-dimethyl, *N*′-methyl, *N*″-methyl pararosaniline ($\lambda_{max} = 573.7$ nm). Intermediate **B** further undergoes demethylation to form intermediate **D** *N*,*N*-dimethyl, *N*′-methyl pararosaniline ($\lambda_{max} = 566.3$ nm), which is also formed from intermediate **C**. Intermediate **C** undergoes demethylation to form intermediate **E** *N*-methyl, *N*′-methyl, *N*″-methyl pararosaniline ($\lambda_{max} = 570.0$ nm). Intermediate **F** *N*-methyl, *N*′-methyl pararosaniline ($\lambda_{max} = 561.3$ nm) is a result of demethylation of **D** or **E**. Further irradiation does not lead to any hypsochromic shift and that leads to complete decolorization, suggesting the destruction in the aromatic conjugates chromophore of *N*-demethylated intermediate. At each step, this *N*-demethylation process is associated with the destruction of conjugative aromatic system of chromophore. When CV was catalyzed by anatase TiO_2 nanorods obtained from hot water treatment, the intermediate **E** was not observed, whereas when it was catalyzed by anatase TiO_2 nanorods obtained from calcination, the mechanism proceeds through the intermediates **A**, **C** and **E**. In other words, tetra-demethylation is not observed with the TiO_2 nanorod catalyst obtained from hot water treatment, contrary to what happens with the anatase TiO_2 nanorods catalyst obtained from calcination. From the results, it is clear that the degradation proceeds through two mechanistic pathways, *N*-demethylation, and the destruction of the conjugated system. The *N*-demethylation process predominates in the initial stage and ring rupture is significant in the later stage.

Conclusion

High surface area titanium glycolate nanorods (TGN) with microporous structure were synthesized from the reaction of titanium alkoxides ($Ti(OEt)_4$, $Ti(O^iPr)_4$, or $Ti(O^nBu)_4$) with ethylene glycol, using a sol–gel reflux method. By hot water treatment at 90 °C of these TGN, mesoporous anatase TiO_2 nanorods were formed, retaining the structural integrity of TGN. High surface areas and pore volumes (480 m^2/g and 1.6 cm^3/g for anatase TiO_2 samples prepared from $Ti(OEt)_4$, 418 m^2/g and 1.6 cm^3/g for anatase TiO_2 samples prepared from $Ti(O^iPr)_4$, and 499 m^2/g and 1.1 cm^3/g for anatase TiO_2 samples prepared from $Ti(O^nBu)_4$) were obtained. When the as-synthesized microporous TGN were calcined at 400 °C, they also transformed into mesoporous anatase TiO_2 nanorods but with a large decrease in the surface area (65 m^2/g for the sample prepared from $Ti(O^nBu)_4$). A mechanism of low temperature crystallization of microporous TGN into mesoporous anatase TiO_2 nanorods is proposed. The hot water prepared mesoporous TiO_2 nanorods should be promising for applications in photocatalysis. When applied to the photodegradation of crystal violet cationic dye (CV), mesoporous anatase TiO_2 nanorods obtained from hot water treatment were found to be a more efficient photocatalyst than anatase titania nanorods obtained by calcination at 400 °C. A mechanism of the photodegradation of CV is presented. From the results, it is clear that the degradation of CV proceeds through two mechanistic pathways, *N*-demethylation, and the destruction of the conjugated system. The *N*-demethylation process predominates in the initial stage and ring rupture is significant in the later stage.

Acknowledgements The financial support of the Research Assistantships Initiative of New Brunswick Innovation Fund (NBIF), the Atlantic Innovation Fund (AIF–Round II), and National Science and Engineering Research Council (NSERC) of Canada is gratefully acknowledged. We thank Dr. Louise Weaver (Microscopy Microanalysis Facility, University of New Brunswick, Fredericton, NB, Canada) for the TEM measurements, and Zoulika Hadj—Sadok (Laboratoire de Chimie des matériaux inorganiques—FUNDP, Namur, Belgique) for BET and XRD measurements. We are also thankful to Dr. Ulrike Werner-Zwanziger, Senior NMR Spectroscopist (Atlantic Magnetic Resonance Center, Department of chemistry, Dalhousie University, Halifax) for the NMR spectra.

References

1. O'Regan B, Gratzel M (1991) Nature 353:737
2. Zhang H, Li GR, An LP, Yan TY, Gao XP, Zhu HY (2007) J Phys Chem 111:6143
3. Djaoued Y, Thibodeau M, Robichaud J, Balaji S, Priya S, Tchoukanova N, Bates SS (2008) J Photochem Photobiol A Chem 193:271
4. Balaji S, Albert A-S, Djaoued Y, Brüning R (2009) J Raman Spectrosc 40:92
5. Quan X, Ruan X, Zhao H, Chen S, Zhao Y (2007) Environ Pollut 147:409
6. Li J, Ma W, Chen C, Zhao J, Zhu H, Gao X (2007) J Mol Catal A Chem 261:131
7. Zhu H, Gao X, Lan Y, Song D, Xi Y, Zhao J (2004) J Am Chem Soc 126:8381
8. Wang D, Yu R, Kumuda N, Kinomura N (1999) Chem Mater 11:2008
9. Wang D, Yu R, Chen Y, Kumuda N, Kinomura N, Takano M (2004) Solid State Ion 172:101
10. Jiang X, Wang Y, Herricks T, Xia Y (2004) J Mater Chem 14:695
11. Yu HK, Eun TH, Yi G-R, Yang S-M (2007) J Colloid Interface Sci 316:175
12. Yu JG, Yu JC, Leung MKP, Ho WK, Cheng B, Zhao XJ, Zhao JC (2003) J Catal 217:69
13. Bavykin DV, Lapkin AA, Plucinski PK, Friedrich JM, Walsh FC (2005) J Catal 235:10
14. Yu JC, Yu JG, Zhao JC (2002) Appl Catal B 36:31
15. Herrmann JM (1999) Catal Today 53:115
16. Cullity BD (1959) Elements of X-ray diffraction. Addison-Wesley Publishing, Reading, MA
17. Balaji S, Djaoued Y, Robichaud J (2006) J Raman Spectrosc 24:247
18. Djaoued Y, Badilescu S, Ashrit PV, Bersani D, Lottici PP, Brüning R (2002) J Sol-Gel Sci Technol 24:254
19. Ohsaka T, Izumi F, Fujiki Y (1978) J Raman Spectrosc 7:321

20. Scott RWJ, Coombs N, Ozin GA (2003) J Mater Chem 13:969
21. Barroso-Bujans F, Martinez R, Ortiz P (2003) J Appl Polym Sci 88:302
22. Zhang D, Qi L (2005) Chem Commun 2735
23. Chae W-S, Lee S-W, Kim Y-R (2005) Chem Mater 17:3072
24. Yu H, Yu J, Cheng B, Lin J (2007) J Hazard Mater 147:581
25. Wang D, Yu R, Kumada N, Kinomura N (1999) Chem Mater 11:220
26. Gröhn F, Bauer BJ, Kim G, Amis E (2001) J Polym Mater Sci Eng 84:78
27. Chen C-C, Fan H-J, Yang C-Y, Jan J-L, Lin H-D, Lu C-S (2006) J Photochem Photobiol A Chem 184:147